Sensors and Actuators A 149 (2009) 233–240

Contents lists available at ScienceDirect

Sensors and Actuators A: Physical

journal homepage: www.elsevier.com/locate/sna

Nanocomposite functional paint sensor for vibration and noise monitoring

Osama J. Aldraihem[a,*], Wael N. Akl[b], Amr M. Baz[c]

[a] Mechanical Engineering, King Saud University, PO Box 800, Riyadh 11421, Saudi Arabia
[b] Design & Production Engineering Department, Ain Shams University, Cairo, Egypt
[c] Mechanical Engineering Department, University of Maryland, 2137 Eng. Bldg., College Park, MD 20742, United States

ARTICLE INFO

Article history:
Received 4 February 2008
Received in revised form 20 October 2008
Accepted 28 October 2008
Available online 27 November 2008

Keywords:
Functional paint sensor
Carbon black nanocomposite
Conducting polymer
Vibration & noise monitoring
Structural health monitoring

ABSTRACT

A new class of nanocomposite functional paint sensor is proposed, whereby an epoxy resin is mixed with carbon black nanoparticles to make the sensor sensitive to mechanical excitations. A comprehensive analysis is presented to understand the underlying phenomena governing the operation of this class of paint sensors. The analysis includes developing an electromechanical model which treats the sensor system as a lumped-parameter system. The Debye and the Cole–Cole equations are utilized to model the behavior of the nanocomposite paint. The sensor equations are integrated with a simple amplifier circuit in order to predict the current and voltage developed by the paint sensor. Several experiments are performed to assess the validity of the proposed models of the paint sensor system. First, impedance spectroscopy is employed to verify the validity of the Debye and Cole–Cole models and to obtain the sensor electrical parameters. Then, experiments are carried out to validate the piezoresistance model. Finally, the predictions of the electromechanical model are experimentally verified by examining the dynamic response of the sensor system under cyclic loading.

The ultimate goal of this study is to demonstrate the feasibility of the proposed nanocomposite functional paint as a sensor for monitoring the vibration, acoustics, and health of basic structural systems.

1. Introduction

Paints are commonly applied as films on structures surfaces for providing protective and decorative functions. When the paint possesses a sensing capability, the paint becomes functional or smart. Recently, several attempts have resulted in the development of smart paints which can be used as sensors for vibration, noise, and health monitoring applications. The currently available functional paints are complex and very expensive for practical applications. For example, smart composite paints which are made of piezoelectric powder immersed in epoxy resin must be coated with layers of electrodes and then poled using very high voltage to impart the sensing capability to the paint [1–3]. Such a complex preparation processes make this type of paint very expensive. Furthermore, expensive charge amplifiers are needed to monitor the capacitive output signals of the smart paint sensor. Alternatively, the pressure sensitive smart paints which modulate the light intensity through a repeatable chemical interaction of the sensing layer with atmospheric oxygen require the use of an expensive photo-detector such as a CCD camera or photomultiplier tube for interrogation of the paint [4].

Carbon black (CB) composite is another class of functional material that finds wide applications, e.g., in deformation sensing. The composite consists basically of electrically conductive CB aggregates embedded in a polymer matrix. The composite conductivity noticeably changes with the applied mechanical deformation.

Extensive research effort has been put forth to studying the percolation theory which is often used to describe the relationship between CB contents and the direct current (DC) conductivity [5]. However, investigation of the sensing ability of CB composites is focused on the detection of quasi-static effect. For example, the work of Shevchenko et al. [6] focused on graphite filled polypropylene composites, which possess smart properties, such as a positive temperature coefficient of resistance and strain dependent conductivity. Along a similar direction, Kimura et al. [7] experimentally illustrated the linear relationship between the logarithms of the resistance and elongation. Furthermore, they developed a model based on the tunneling junction model. Flandin et al. [8] evaluated the DC electrical and mechanical properties of composites composed of conductive fillers impeded into elastomer matrices. Zhang et al. [9] presented a systematic work on the piezoresistance effects of electrically conducting composites which are subject to uni-axial pressure. The investigation experimentally verified the theoretical

* Corresponding author. Tel.: +966 1 4670166.
E-mail addresses: odraihem@ksu.edu.sa (O.J. Aldraihem), waelakl@gmail.com (W.N. Akl), baz@eng.umd.edu (A.M. Baz).

0924-4247/$ – see front matter © 2008 Elsevier B.V. All rights reserved.
doi:10.1016/j.sna.2008.10.017

model for the piezoresistance. In another work, Zhang et al. [10] extended their former investigation to study the time dependence of the piezoresistance. Knite et al. [11] proposed the use of carbon black nanocomposites as tensile strain and pressures sensor. The investigation included experimental results and a theoretical model based on that of Zhang et al. [9]. In a recent work, Wang et al. [12] studied the conduction mechanism in CB composites using impedance spectroscopy. Three equivalent-circuit models are proposed for the various regions of percolation theory curve. Another group of investigators [13,14] studied the piezoresistive behaviors of graphite composites under static pressures. Das et al. [15] is focused on the variation of the resistivity of CB and short carbon fiber composites with the degree of strain at constant strain rate.

In this work, a nanocomposite paint is proposed whereby an epoxy resin is mixed with carbon black nanoparticles to make it act as a functional composite. The paint sensor is very simple and capable of monitoring vibration and noise down to a quasi-static frequency of ≈0 Hz. Accordingly, simple electrical circuits can be used to measure the changes in the current and voltage developed by the paint sensor.

It is also important to mention that the proposed paint can be easily applied to structures of complex shapes and can act as a continuously distributed sensor over very large areas of structural surfaces. The proposed paint sensor can be used in numerous applications ranging from monitoring infrastructures, payload fairings of launching vehicles, flexible space structures, as well as many other critical structures that are only limited by our imagination.

In the present study, the objective is to develop a comprehensive model of the paint sensor system for vibration, noise, and health monitoring applications. A lumped-parameter approach is used to obtain the paint sensor equations. Furthermore, impedance equations are presented to estimate the electrical parameters of the paint sensor. Hamilton's principle for electromechanical systems is employed to derive the dynamic equations of the sensor system. The developed models are verified experimentally by examination of the impedance spectrum, piezoresistance, and dynamic response.

The paper is organized in four sections. Section 1 briefly summarizes the literature review. In Section 2, the equivalent circuit model of the functional paint is developed using the Debye and Cole–Cole equations. Then, estimates of the paint electrical components are obtained from the impedance equations. An electromechanical model is derived for the paint sensor system using the Hamilton's principle. The model is based on an equivalent circuit representation which treats the real sensor system as a lumped-parameter system. The sensor system equations are integrated with a simple electrical circuit to enable the measurement of the current and voltage developed by the functional paint sensor. Section 3 presents experimental validations of the predictions of the developed models and provides assessments of the static and dynamic performance characteristics of the paint sensor system. Section 4 summarizes the major conclusions and recommendations of the present study.

2. Model development

2.1. Nanoparticle paint sensor

The proposed paint sensor is a conductive composite, as shown in Fig. 1, whereby a polymer resin is mixed with CB aggregates to make it electrically conducting and functional.

The geometric scale of the aggregate can, in general, range from nanoscale to microscale. Furthermore, the composite sensor is assumed to be homogeneous on the macroscale.

To facilitate modeling formulation, the real microstructure of the sensor is simplified as illustrated in Fig. 2. The primary aggregates consist of many CB nanoparticles, where each CB aggregate

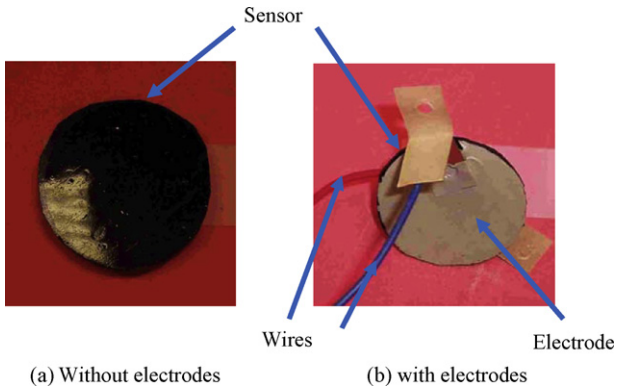

Fig. 1. Sample of a paint sensor.

is assumed to form a continuum phase of a spherical shape. Moreover, each CB aggregate possesses high-structure of high electrical conductivity. The weight fraction loading of the carbon black phase is assumed to be within the percolation region.

The principle of sensing can be best understood by considering the schematic circuit shown in Fig. 2. This circuit enables the measurement of the current and/or voltage developed by the paint sensor. A voltage source, u_{in}, along with a series resistor, R_0, is used to bias the sensor. When the sensor is subject to external vibration or acoustic excitations, its electrical properties are altered and so are the current and voltage of the bias resistor. The resulting changes are proportional to the external excitations. The representation of Fig. 2 illustrates the basic configuration of the sensor measurement system that can be used as load (force, pressure) and/or deformation (displacement, strain, velocity, etc.) sensor.

2.2. Equivalent lumped-parameter models

The paint sensor is basically an electromechanical transducer which can be described by the constitutive (characteristic) equations of the sensor and the equations of motion of sensor structure along with the associated boundary conditions. The equivalent lumped-parameter approach can be used to replace the system governing equations with a lumped-parameter electrical circuit whose elements physically represent the sensor electromechanical properties such as the capacitance, resistance, mass, stiffness, and damping [16]. The equivalent circuit method is attractive in the sense that the sensor system can be cast in a single representation. Furthermore, the equivalent circuit method is often used to model and analyze coupled domain devices including electrostatic transducers [17], piezoelectric devices [18], ionic polymer [19], and electroacoustic devices [20].

In what follows, the equivalent lumped-parameter approach will be used to obtain the paint sensor equations.

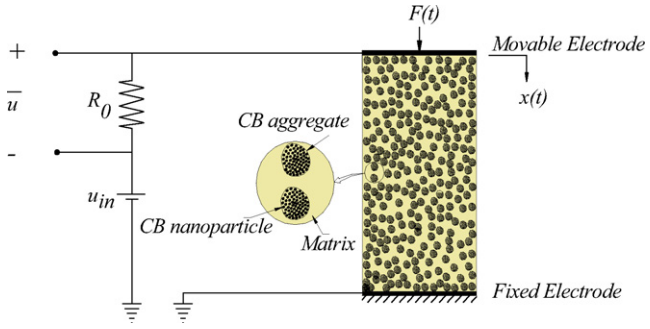

Fig. 2. Schematic circuit of the sensor.

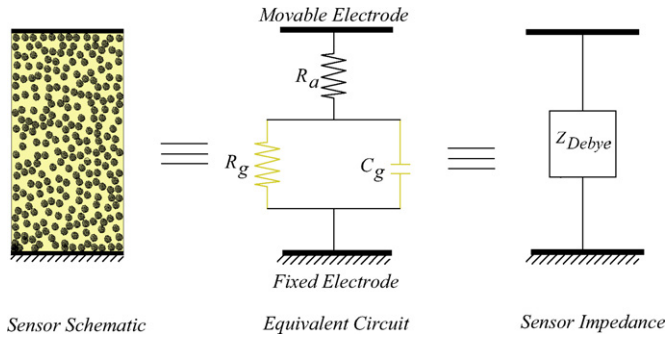

Fig. 3. Equivalent electrical circuit of the ideal, Debye, model.

2.2.1. Ideal components, Debye model

The simplest equivalent circuit mimicking the impedance of electrically conducting composites can be modeled by a Debye equation. The equivalent circuit of this model consists of a resistance, R_a, connected in series with parallel R_g–C_g elements [12], as shown in Fig. 3. The resistance R_a is the overall carbon black aggregates resistance of the composite. The gaps between the carbon black aggregates are equivalent to resistor–capacitor elements. These parallel elements R_g and C_g are the overall gaps resistance and capacitance of the composite, respectively. The R_a, R_g and C_g components are considered ideal, that is frequency independent, and are estimated from the impedance spectrum of the sensor. The frequency dependent impedance of this composite sensor is

$$Z_{\text{Debye}} = R_a + \frac{R_g}{1 + j\omega\tau} \tag{1}$$

with

$$\tau = R_g C_g, \quad j = \sqrt{-1} \tag{2}$$

where $\omega(=2\pi f)$ is the angular frequency and τ is the characteristic time of the equivalent circuit. The real and imaginary parts of the Debye impedance (1) can be extracted, respectively, as

$$\begin{aligned} Z'_{\text{Debye}} &= R_a + \frac{R_g}{1 + (\omega\tau)^2} \\ Z''_{\text{Debye}} &= -\frac{\omega R_g \tau}{1 + (\omega\tau)^2} \end{aligned} \tag{3}$$

The ideal components R_a, R_g and C_g can be estimated from the values of Z'_{Debye} and Z''_{Debye}. At low frequency, the value of the real part is $R_a + R_g$, however, this value reduces to R_a at very high frequency. When the frequency reaches $(1/\tau)$, the imaginary part attains a maximum value of $Z''_{\max} = Z''_{\text{Debye}}(\omega_{\max} = (1/\tau)) = -(R_g/2)$. At this frequency, $\omega_{\max}$, the capacitance of the composite can be calculated via $C_g = (1/(R_g\omega_{\max}))$.

2.2.2. Frequency dependent components, Cole–Cole model

The Debye model presented in the previous section is useful in describing a composite sensor with impedance possessing frequency independent parameters. When the matrix of the composite sensor is made of polymer, the impedance parameters become frequency dependent. For such a case, a good representation can be obtained by the Cole–Cole empirical equation:

$$Z_{\text{C–C}} = R_a + \frac{R_g}{1 + (j\omega\tau)^\alpha} \tag{4}$$

where α is a dimensionless positive parameter with values in the range, $1 \geq \alpha \geq 0$. Using *De Moivre* identity, $j^\alpha = \cos(\alpha\pi/2) + j\sin(\alpha\pi/2)$, the impedance (4) is expanded as

$$Z_{\text{C–C}} = R_a + \frac{R_g}{1 + \omega^\alpha\tau^\alpha \cos(\alpha\pi/2) + j\omega((\omega^\alpha/\omega\tau^\alpha)\sin(\alpha\pi/2))} \tag{5}$$

Letting $\tau = R_g^{1/\alpha} C_g$, the impedance (5) is reduced to

$$Z_{\text{C–C}} = R_a + \frac{1}{(1/R_g) + (1/r_\omega) + j\omega c_\omega} \tag{6}$$

with frequency dependent resistor and capacitor given by

$$\begin{aligned} r_\omega &= \frac{1}{\omega^\alpha C_g^\alpha \cos(\alpha\pi/2)} \\ c_\omega &= \frac{\omega^\alpha}{\omega} C_g^\alpha \sin(\alpha\pi/2) \end{aligned} \tag{7}$$

where R_a, R_g and C_g are frequency independent elements. The real and imaginary parts take form similar to those of the Debye model (3) and are given, respectively, as

$$\begin{aligned} Z'_{\text{C–C}} &= R_a + \frac{R_e}{1 + (\omega\tau_w)^2} \\ Z''_{\text{C–C}} &= -\frac{\omega R_e \tau_\omega}{1 + (\omega\tau_w)^2} \end{aligned} \tag{8}$$

where

$$\tau_\omega = R_e c_\omega, \quad R_e = \frac{R_g r_\omega}{R_g + r_\omega} \tag{9}$$

The equivalent circuit of the Cole–Cole impedance (6) can be represented graphically, as shown in Fig. 4. In Cole–Cole model, four parameters should be estimated; R_a, R_g, C_g and α. The dimensionless positive number α is obtained from fitting the data. The components R_a, R_g and C_g can be estimated from the values of $Z'_{\text{C–C}}$ and $Z''_{\text{C–C}}$. For $\alpha = 1$, it should be clear that the resistor term in (6), $1/r_\omega$, vanishes and the capacitor, c_ω, becomes C_g leading to the Debye model.

2.3. Governing equations of the sensor system

The sensor system depicted in Fig. 2 is modeled as shown in Fig. 5. This model is a lumped-parameter model which treats the mechanical domain as a single degree of freedom system. The circuits shown in Figs. 3 and 4 are adopted for the sensor electrical domain. Depending on the model used, the sensor impedance, Z_s, can be taken from the Debye (1) or the Cole–Cole (6) equation. The mechanical elements are the equivalent mass, m, the equivalent stiffness, K, and the equivalent damping coefficient, b. When the sensor is disturbed by a force $F(t)$, the mass is displaced by an amount $x(t)$. The mechanical disturbance is converted into electrical current signal which flows in part through the resistor, R_0, thereby changing the output voltage $\tilde{u}(t)$. This voltage is considered as measure for the force or velocity.

When the sensor is electrically and mechanically unloaded, the distance between the two electrodes is x_0. But, when the sensor is subjected to only a DC bias voltage, the bias voltage generates an attractive force between the electrodes and an equilibrium state

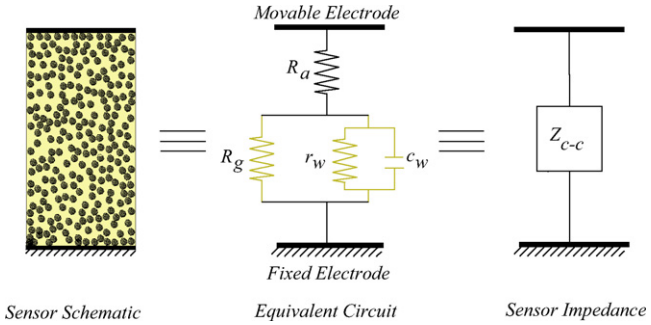

Fig. 4. Equivalent electrical circuit of the Cole–Cole model.

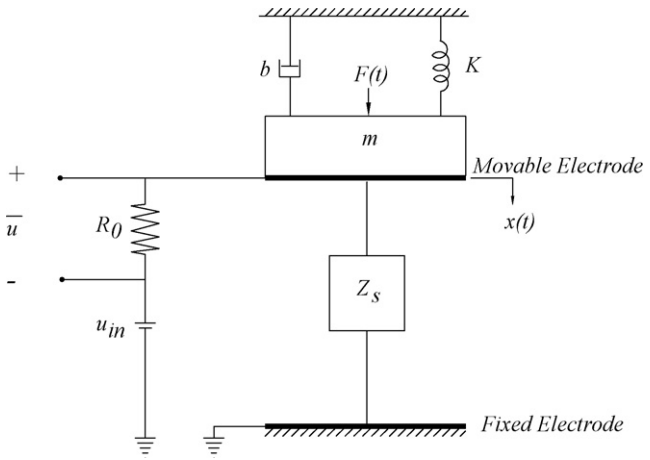

Fig. 5. Lumped-parameter representation of the paint sensor system.

is attained. At the equilibrium state, the two electrodes are separated by a distance x_{dc}, and the sensor is deformed by a distance $d = x_0 - x_{dc}$. The equilibrium distance x_{dc} is obtained by balancing the sensor stiffness force with the electrostatic force of the dc bias. This is derived as

$$Kd = \frac{Q_{dc}^2}{2\varepsilon A} \Rightarrow x_{dc} = x_0 - \frac{Q_{dc}^2}{2K\varepsilon A} \tag{10}$$

where Q_{dc} denotes the charge in the sensor electrodes due to dc bias, ε denotes the effective permittivity of the sensor, and A denotes the area of the electrodes.

Hamilton's principle for electromechanical systems will be used to derive the governing equations of the sensor system. In the interest of simplicity, the derivation will only consider the Debye equivalent circuit of the sensor as shown in Fig. 6. Hamilton's principle yields the following Lagrange's equation for the electromechanical systems [21].

$$\begin{aligned} &\frac{d}{dt}\left(\frac{\partial L}{\partial \dot{z}_i}\right) + \frac{\partial D}{\partial \dot{z}_i} - \frac{\partial L}{\partial z_i} = P_i \\ &\text{and} \quad \frac{d}{dt}\left(\frac{\partial L}{\partial \dot{\bar{Q}}_k}\right) + \frac{\partial D}{\partial \dot{\bar{Q}}_k} - \frac{\partial L}{\partial \bar{Q}_k} = E_k \end{aligned} \tag{11}$$

with the Lagrangian given by

$$L = T^* - V - W_e \tag{12}$$

The Lagrangian (12) accounts for all the conservative elements in the system and

$$\delta W_{nc} = \sum_{i=1}^{n} P_i \delta z_i + \sum_{k=1}^{l} E_k \delta \bar{Q}_k \tag{13}$$

is the virtual work of all non-conservative elements. Where P_i includes all the non-conservative mechanical loads which are not accounted for in the dissipation function, and E_k denotes the non-conservative voltage.

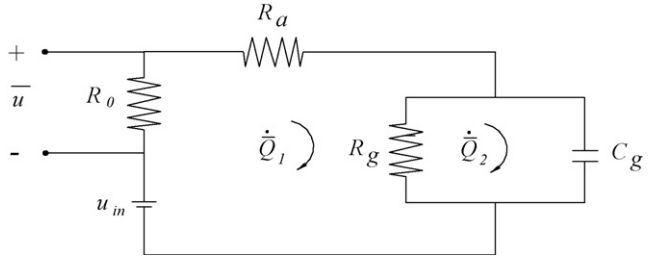

Fig. 6. Electrical circuit of the sensor system.

With reference to Fig. 6, the electrical charges in the sensor system are given by

$$\begin{aligned} &\bar{Q}_1(t) = Q_{1dc} + Q_1(t) \\ &\text{and} \quad \bar{Q}_2(t) = Q_{2dc} + Q_2(t) \end{aligned} \tag{14}$$

where Q_{idc} ($i = 1, 2$) is the charge due to a DC bias and $Q_i(t)$ is the charge created by the excitation.

For Debye model, the various energy contributions to the Lagrangian are

$$\begin{aligned} &T^* = \frac{1}{2} m\dot{x}^2, \\ &V = \frac{1}{2} K(x+d)^2, \\ &\text{and} \quad W_e = \frac{1}{2C_g}\bar{Q}_2^2. \end{aligned} \tag{15}$$

where T^* is the kinetic energy, V is the potential energy, and W_e is the electrical energy of the sensor system.

With reference to Figs. 5 and 6, the dissipation energy function is given as

$$D = \frac{1}{2}\left(b\dot{x}^2 + (R_0 + R_a)\dot{\bar{Q}}_1^2 + R_g\left(\dot{\bar{Q}}_1 - \dot{\bar{Q}}_2\right)^2\right) \tag{16}$$

and

$$\delta W_{nc} = F(t)\delta x + u_{in}\delta \bar{Q}_1 \tag{17}$$

The capacitance of the overall gap, C_g, varies with displacement of the movable electrode about the equilibrium position according to

$$C_g = \frac{\varepsilon A}{x_{dc} - x(t)} \tag{18}$$

Furthermore, the overall gaps resistance R_g varies with the sensor deformation according to [9]

$$R_g = R_{gdc}\left(1 - \frac{x(t)}{x_{dc}}\right) e^{-\gamma s_0 (x(t)/x_{dc})} \tag{19}$$

with

$$\gamma = \frac{4\pi}{h}\sqrt{2m_e\varphi} \tag{20}$$

$$s_0 = D\left(\sqrt[3]{\frac{\pi}{6\theta}} - 1\right) \tag{21}$$

where R_{gdc} is the overall gap resistance at equilibrium, D is the CB aggregate diameter, θ is the CB volume fraction, h is the Plank constant, m_e is the electron mass, and φ is the height of the potential barrier between adjacent carbon black aggregates.

Using Eqs. (14)–(18) in the Lagrange's Eq. (11) and carrying out some mathematical manipulations yields the governing equations.

$$\begin{aligned} &m\ddot{x} + b\dot{x} + Kx - \frac{Q_{2dc}}{\varepsilon A}Q_2 = F, \\ &(R_0 + R_a)\dot{Q}_1 - R_g(\dot{Q}_2 - \dot{Q}_1) = 0, \\ &\text{and} \quad R_g(\dot{Q}_2 - \dot{Q}_1) + \frac{x_{dc}}{\varepsilon A}Q_2 - \frac{Q_{2dc}}{\varepsilon A}x = 0. \end{aligned} \tag{22}$$

The above Eq. (22) represents the nonlinear dynamic behavior of the sensor system. The nonlinearity is seen in the terms containing R_g where $x(t)$ is embedded. The displacement, $x(t)$, is coupled with the electrical charge $Q_2(t)$ via the electromechanical coupling factor $(Q_{2dc}/\varepsilon A)$. Furthermore, the displacement, $x(t)$ which is hidden in the R_g terms, can affect the electrical response of the system.

In general, the output voltage drop in the resistor R_0 and the voltage across the paint sensor are available for measurement. Since

they differ only by the excitation voltage, which is known u_{in}, it is sufficient to consider only one of them. The voltage drop in the resistor R_0 is given as

$$\bar{u} = R_0 \dot{\bar{Q}}_1 \tag{23a}$$

or

$$\bar{u} = u_{dc} + u(t) = R_0 \dot{Q}_{1dc} + R_0 \dot{Q}_1 \tag{23b}$$

The first term in (23b) is the voltage drop in the resistor at equilibrium, while the second term is due to the mechanical excitation. Solving the system (22) for a given excitation $F(t)$ provides solutions for $x(t)$, $Q_1(t)$, $Q_2(t)$ and their derivatives. This solution set can readily be used to obtain $u(t)$ and $\bar{u}$.

2.4. Mechanical elements

The mechanical elements of the composite sensor are represented in Fig. 5 by K, m, and b. For an axial bar, an expression for the mechanical equivalent stiffness can be derived by considering the quasi-static relationship between applied force and the produced deformation. For small deformations, the axial load and the deformation are related through

$$F = \frac{E'A}{x_0} x \tag{24}$$

with [22]

$$E' = E'_p \left(1 + 2.5\phi + 14.1\phi^2\right) \tag{25}$$

where E' is the sensor elastic (storage) modulus (the elastic modulus of the composite sensor is complex due to the polymer matrix), E'_p is the elastic (storage) modulus of the polymer matrix, and ϕ is the volume fraction of the CB filler.Eq. (24) leads to the sensor equivalent stiffness

$$K = \frac{E'A}{x_0} \tag{26}$$

Similarly, the equivalent mass of the sensor is obtained for composite bar. This is achieved by combining the quasi-static bar stiffness with the bar's natural frequency. For axial vibration, the fundamental frequency of a fixed-free bar is

$$\omega = \frac{\pi}{x_0}\sqrt{\frac{E'}{\rho}} \tag{27}$$

where ρ is the composite sensor density. This density can be estimated by using the rule of mixture.

For a one degree of freedom system the relationship

$$\omega = \sqrt{\frac{K}{m}} \tag{28}$$

can be used to estimate the equivalent mass of the paint sensor. Solving Eqs. (26)–(28) for the equivalent mass yields

$$m = \frac{4x_0}{\pi^2}\rho A \tag{29}$$

Finally, the damping term is derived using the damping the complex modulus $E = E' + jE''$ of the composite sensor and the relationship [23]

$$\omega = \eta \frac{K}{b} \tag{30}$$

with the lost factor

$$\eta = \frac{E''}{E'} \tag{31}$$

where E'' denotes the loss modulus.

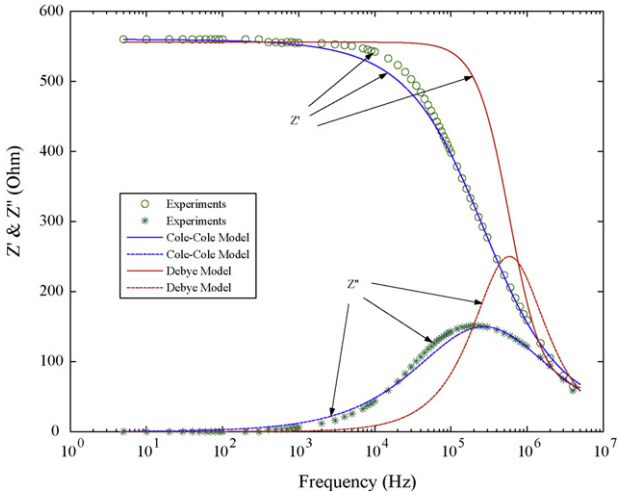

Fig. 7. Real Z' and imaginary Z'' impedance spectrum.

Table 1
Estimated electrical parameters of equivalent circuits (mechanically unloaded).

Model	R_g (Ω)	R_a (Ω)	C_g ($\times 10^{-11}$ F)	α
Debye				
50 mV excitation	500	56	54.332	–
Cole–Cole				
50 mV excitation	540	20	3.4332	0.645
3 V excitation	485	15	3.461	0.655

The equivalent damping coefficient is obtained by solving Eqs. (26), (27) and (30).

$$b = \frac{2}{\pi}\eta A\sqrt{\rho E'} \tag{32}$$

It should be mentioned that Eq. (25) is also applicable to determine the loss modulus (E'', E''_p instead of E' and E'_p, respectively).

3. Models verification

3.1. Impedance spectrum

To obtain quantitative information from the sensor model presented in Section 2.3, one must first determine values for several electrical parameters. Experimental impedance spectroscopy is employed in this work to verify the validity of the Debye and

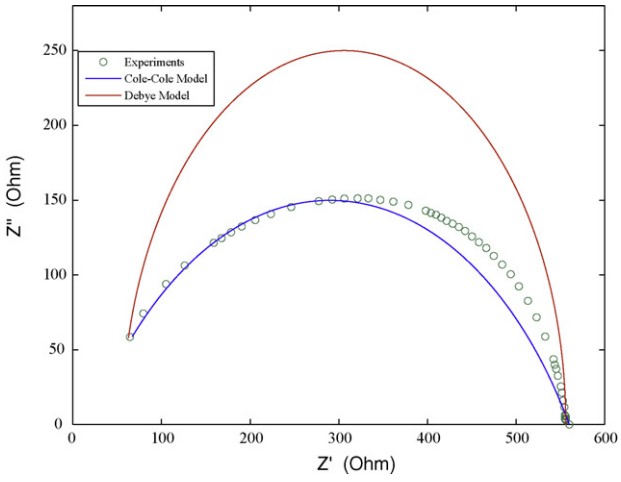

Fig. 8. Complex impedance spectrum.

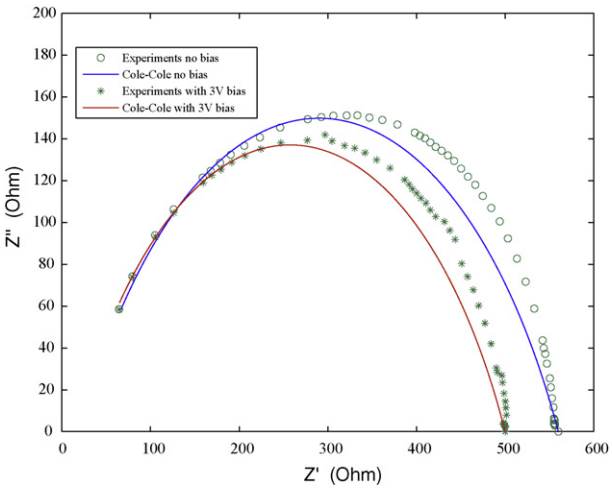

Fig. 9. Complex spectrum of a sensor biased by a signal with amplitude of 3 V.

Cole–Cole models and to obtain the electrical parameters. All of the experiments were performed on a paint sensor which consists of 10 wt% CB aggregates embedded in a polyurethane matrix. A Tissue Tearor mixer (Model 985370, BIOSPEC Products, Inc., Bartlesville, OK (http://www.biospec.com) is used to ensure the homogeneity of the paint.

The CB used was acetylene black, from Alfa Aesar Company, with an average particle size 42-nm, a surface area 75 m^2/g, a density 2.26 g/cm^3 and a bulk density 94.5–102.5 kg/m^3 [24]. The matrix used was 60A polyether-based urethane, from Forsch Polymer Corp., with a density 1.08 g/cm^3 and an elastic modulus 2–3.8 MPa [25]. The loss factor of the urethane is 0.12, which was obtained experimentally. The relative dielectric constant of the urethane is 5.0–8.8 [26].

Samples were fabricated by hand mixing the urethane and CB and pouring the mixture in a metal mold for one day. The samples were then cut into disk shape, coated with surface electrodes made of conductive silver paint, and connected with leads. The samples were 24.6-mm diameter and 0.942-mm average thickness.

The impedance spectra were measured at room temperature using impedance analyzer, Hewlett Packard 4192A LF, over the frequency range from 5 Hz to 4 MHz. The analyzer was set on a series mode, and the samples were excited by a signal with amplitude of 50 mV.

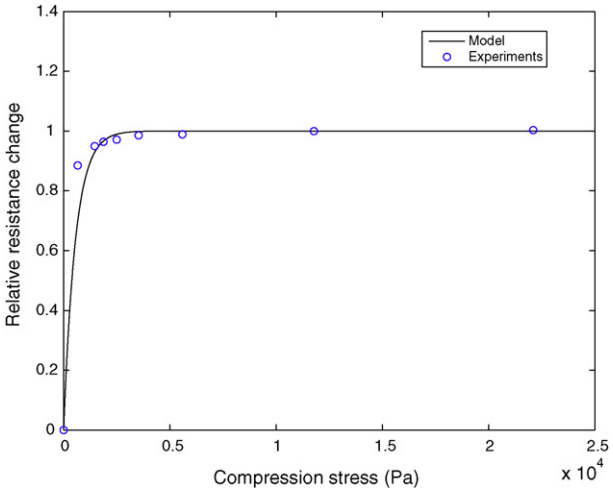

Fig. 10. Measured and predicted relative resistance change.

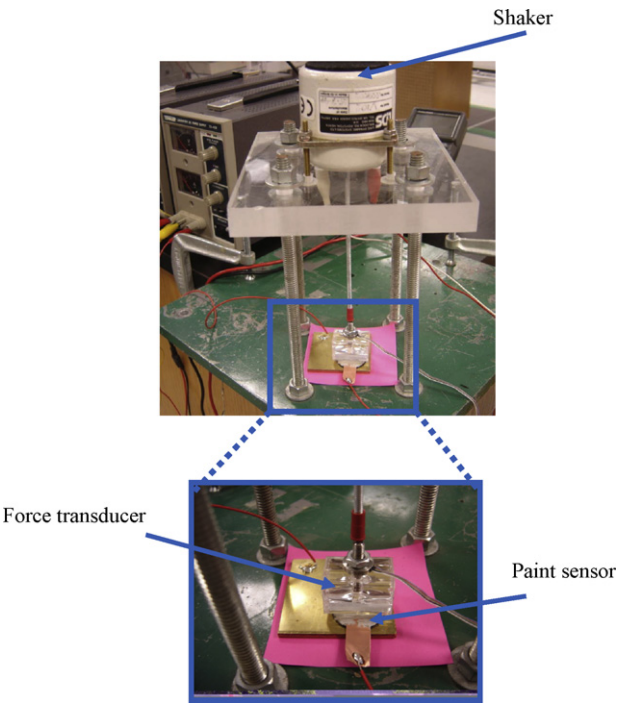

Fig. 11. Experimental set-up for the dynamic response.

Fig. 7 shows the real Z' and imaginary Z'' impedance spectrum in the frequency range from 5 to 4×10^6 Hz. The figure contains plots from the experiments, Debye and Cole–Cole models. The Debye curves are calculated using Eq. (3) and values of R_a, R_g and C_g that best fit the experimental data and as described in Section 2.2.1. Similarly, the Cole–Cole spectra are determined using Eq. (8) and values of R_a, R_g, C_g and α that best match the experiments and as described in Section 2.2.2. The evaluated values of the parameters are given in Table 1. When compared to the experimental results, it is observed that the Debye model provides good predictions for frequency range less than 1 kHz. On the other hand, the Cole–Cole predictions agree quite well with the experimental results for all frequencies. Furthermore, Fig. 7 shows that the imaginary impedance Z'' is close to zero at frequency below one kHz. This indicates that the current bypasses C_g and flows only thru R_g branch.

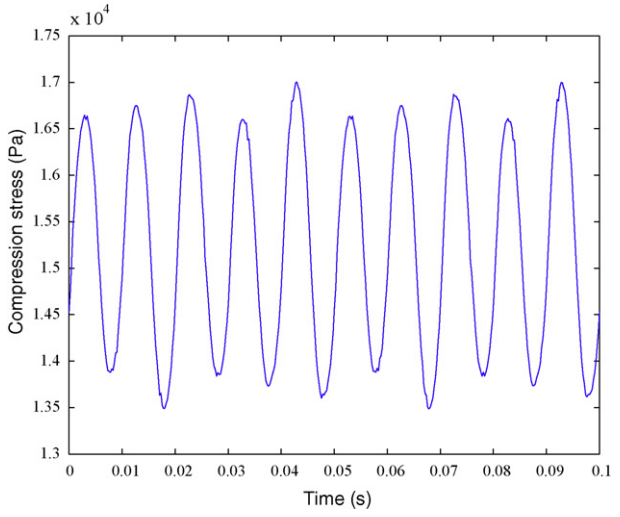

Fig. 12. The applied dynamic stress.

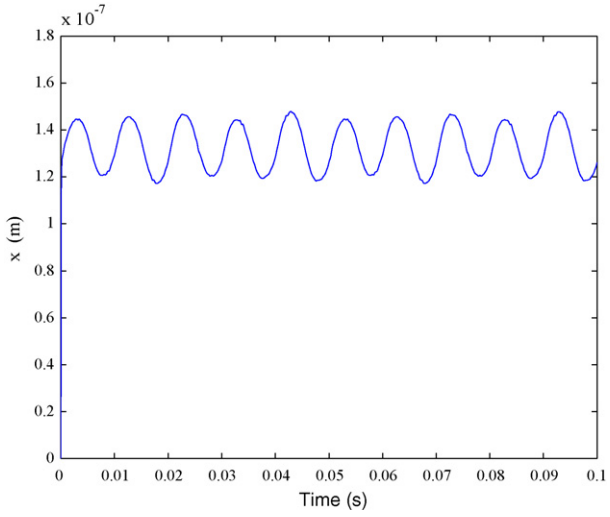

Fig. 13. Predicted displacement $x(t)$ of the movable electrode.

To further confirm the validity of the models, the results are plotted in the complex impedance spectrum as shown in Fig. 8. Here again the Cole–Cole results agree well with those of the experiments, while the Debye curve matches the experimental data only at low and very high frequencies.

Since the proposed sensor system operates under the influence of an external DC excitation, the effect of a DC bias on the impedance spectrum is also investigated. Fig. 9 shows the complex spectrum of a paint sensor biased by a signal with amplitude of 3 V. At low frequency, it can be seen that the presence of a bias voltage reduces the values of R_a and R_g when compared with those of an unbiased sensor. The bias voltage creates attractive force between adjacent aggregates which decreases the separation distance and the sensor resistance. At very high frequency, the bias voltage has no effect on the impedance.

3.2. Piezoresistance

The paint sensor described in Section 3.1 is used here to verify the piezoresistance model (19). The sensor is subjected to compressive stresses created by weights, and the sensor resistance was measured by a digital multimeter. Fig. 10 shows the measured and the predicted relative resistance change as function of the applied stress. Clearly, the predicted results are in good agreement with the experiments verifying the validity of the model (19). At small applied stress, the results show that the relative resistance varies almost linearly with the compression stress.

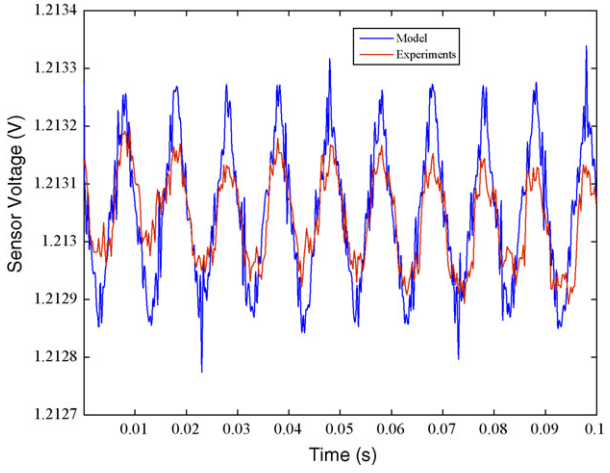

Fig. 14. Predicted and experimental voltages drop in the sensor.

3.3. Dynamic response

The dynamic model (22) of the paint sensor system is solved numerically and verified experimentally. The experimental measurements are performed using the test set-up shown in Fig. 11. The paint sensor sample is identical to that described in Section 3.1. The sensor is subjected to a uniaxial dynamic stress which is generated by a shaker. The applied stress is a compression–compression cycling with oscillation frequency of 100 Hz, as shown in Fig. 12. It should be mentioned this low excitation frequency is considered to assure the accuracy of the Deybe model which is used in the dynamic model. A voltage source, $u_{in} = 3$ V, and a series resistor, $R_0 = 560\ \Omega$, are used to bias the sensor. The dynamic response of the sensor is measured via reading of the AC voltage developed in the sensor.

The predicted response of the sensor is obtained by solving the Eq. (22) with input force $F(t)$ identical to that of experiments. The Runge–Kutta method is used to numerically determine the solutions for $x(t)$ and the voltage drop in the sensor.

Fig. 13 shows the predicted displacement $x(t)$ of the movable electrode. The displacement curve contains two parts; a constant displacement caused by the initial compression stress and a fluctuating displacement created by the dynamic cycling. The displacement profile precisely follows that of the applied stress.

Fig. 14 shows the predicted and experimental voltages drop in the sensor. It is observed that the calculated voltage reasonably matches the experimental values. However, the model results slightly overestimate the sensor voltage in particular at the peaks. It is believed this difference in results is due to model assumptions. The model ignores the effects of the applied load on the resistance R_a. Furthermore, the model treats each CB aggregate as a continuum phase of a spherical shape which is not true.

4. Conclusions

The electromechanical model developed in this work provides physically valuable and compact means of analyzing a new class of functional paint sensor. The model describes the paint sensor as a resistance connected in series with parallel *RC* elements. The impedance of the sensor possesses frequency independent or dependent parameters depending on the considered model: Debye or Cole–Cole equation. The electrical impedance expression is beneficial for the estimation of the sensor electrical parameters. The model formulation exploits the capacitance element in the equivalent circuit to develop the electromechanical constitutive equations; hence, the electromechanical coupling is similar to the one used for electrostatic systems. The equivalent circuit analysis of the sensor system reveals nonlinear relationships between the electrical and mechanical variables. The nonlinearity is caused by the gap resistance. The sensor system equations offer straightforward relations between the mechanical excitation inputs (force, velocity or displacement) and the electrical output signals (voltage or current).

The experiments presented, in this work, demonstrate the validity of the proposed models for both the functional paint and the sensor system. The results verify the validity and applicability of the Debye and Cole–Cole equation to estimate the electrical parameters. Furthermore, the results show that the Debye equation can reasonably mimic the paint sensor for frequency below 1 kHz as shown in Fig. 7. The Cole–Cole model can predict the sensor behavior for all frequencies although it is relatively arduous to work with

(Figs. 7–10). The experiments illustrate also the accuracy of the piezoresistance model. Finally, the dynamic response is calculated numerically and verified experimentally by examining the sensor outputs under cyclic loading.

Future investigation should include optimization of the design parameters and ingredients of the functional paint, and experimental evaluation of the merits and limitations such as the band width and drift of the proposed paint. Among the important parameters that should also be considered are the properties of the epoxy resin, mixing ratios of the different ingredients, powder particle sizes, the curing parameters of the paint, the thickness of the paint layer, and the spray parameters. The evaluation of the effect of these parameters on the performance of the sensor is a natural extension of the present work and is a subject to an extensive study.

It is envisioned that the theoretical and experimental techniques presented in this paper will provide the foundation for developing paint sensors for numerous applications ranging from monitoring infrastructures, payload fairings of launching vehicles, flexible space structures, as well as many other critical structures that are only limited by our imagination.

Acknowledgements

The supports, which are provided by the KACST and KSU for nanotechnology research to the researchers of the universities Kingdom of Saudi Arabia, are gratefully acknowledged by the first author.

References

[1] S. Egusa, N. Iwasawa, Piezoelectric paints as one approach to smart structural materials with health-monitoring capabilities, Smart Materials and Structures 7 (1998) 438–445.
[2] Y. Zhang, Piezoelectric paint sensor for real-time structural health monitoring Paper # 5765-121, in: M. Tomizuka (Ed.), Sensors and Smart Structures Technologies for Civil, Mechanical, and Aerospace Systems Conference, SPIE vol. #5765, San Diego, CA, 7–10 March, 2005.
[3] J.M. Hale, J.R. White, R. Stephenson, F. Liu, Development of piezoelectric paint thick-film vibration sensors, Proceedings of The Institution of Mechanical Engineers Part C: Journal of Mechanical Engineering Science 219 (2005) 1–9.
[4] J.W. Gregory, J.P. Sullivan, S.S. Wanis, N.M. Komerath, Pressure-sensitive paint as a distributed optical microphone array, Journal of the Acoustical Society of America 119 (January (1)) (2006) 251–261.
[5] E.K. Sichel, Carbon Black-Polymer Composites, Marcel Dekker, New York, 1982.
[6] V.G. Shevchenko, A.T. Ponomarenko, C. Klason, Strain sensitive polymer composite material, Smart Materials and Structures 4 (1995) 31–55.
[7] T. Kimura, N. Yoshimura, T. Ogiso, K. Maruyama, M. Ikeda, Effect of elongation on electric resistance of carbon-polymer systems [I], Polymer 40 (1999) 4149–4152.
[8] L. Flandin, A. Chang, S. Nazarenko, A. Hiltner, E. Baer, Effect of strain on the properties of an Ethlene–Octene elastomer with conductive carbon fillers, Journal of Applied Polymer Science 76 (2000) 894–905.
[9] X.-W. Zhang, Y. Pan, Q. Zheng, X.S. Yi, Piezoresistance of conductor filled insulator composites, Polymer International 50 (2001) 229–236.
[10] X.-W. Zhang, Y. Pan, Q. Zheng, X.S. Yi, Time dependence of piezoresistance for conductor-filled polymer composites, Journal of Applied Polymer Science Part B: Polymer Physics 38 (2000) 2739–2749.
[11] M. Knite, V. Teteris, A. Kiploka, J. Kaupuzs, Polyisoprene–carbon black nanocaomposites as tensile strain and pressure sensor materials, Sensors and Actuators A: Physical 110 (2004) 142–149.
[12] Y.-J. Wang, Y. Pan, X.-W. Zhang, K. Tan, Impedance spectra of carbon black filled high-density polyethylene composites, Journal of Applied Polymer Science 98 (2005) 1344–1350.
[13] J. Lu, X. Chen, W. Lu, G. Chen, The piezoresistive behaviors of polyethylene/foliated graphite nanocomposites, European Polymer Journal 42 (2006) 1015–1021.
[14] S. Moshfegh, N.G. Ebrahimi, Strain sensors based on graphite fillers, Iranian Polymer Journal 13 (2004) 113–119.
[15] N.C. Das, T.K. Chaki, D. Khastgir, Effect of axial stretching on electrical resistivity of short carbon fibre and carbon black filled conductive rubber composites, Polymer International 51 (2002) 156–163.
[16] H.A.C. Hilmans, Equivalent circuit representation of electromechanical transducers. I. Lumped-parameter systems, Journal of Micromechanics and Microengineering 6 (1996) 157–176.
[17] R. Nadal-Guardia, A.M. Brosa, A. Dehe, AC transfer function of electrostatic capacitive sensors based on the 1D equivalent model: application to silicon microphones, Journal of Micromechanical Systems 12 (2003) 972–978.
[18] T. Ikeda, Fundamental of Piezoelectricity, Oxford Press, New York, 1996.
[19] K.M. Newbury, D.J. Leo, Linear electromechanical model of ionic polymer transducers. Part I. Model development, Journal of Intelligent Systems and Structures 14 (2003) 333–342.
[20] M. Rossi, Acoustics and Electroacoustics, Artech House, Norwood, MA, 1988.
[21] A. Preumont, Mechatronics: Dynamics of Electromechanical and Piezoelectric Systems, Springer, The Netherlands, 2006.
[22] J.-F. Zhang, X.-S. Yi, Dynamic rheological behavior of high-density polyethylene filled with carbon black, Journal of Applied Polymer Science 86 (2002) 3527–3531.
[23] D.J. Inman, Engineering Vibration, 3rd edition, Pearson Education, New York, 2007.
[24] Alfa Aesar, Research Chemicals Metals and Materials Catalogue, A Johnson Mattey Company, Ward Hill, MA, 2003–2004.
[25] Forsch Polymer Corp., Data Sheet, Englewood, CA, www.forschpolymer.com.
[26] I. Diaconu, D. Dorohoia, Properties of polyurethane thin films, Journal of Optoelectronics and Advanced Materials 7 (2005) 921–924.

Biographies

Osama J. Aldraihem (http://faculty.ksu.edu.sa/OAldraihem/default.aspx) obtained his Ph.D. in Mechanical Engineering from State University of New York at Buffalo in 1997. He is associate professor of Mechanical Engineering at King Saud University in Saudi Arabia. Since 2004, he is serving as the vice dean for technical affairs in the deanship of scientific research. During the period 2003–2004, he served as the Director of Research Center at the College of Engineering. His research interests cover all aspects of smart materials and structures. He has published more than 30 articles in referred journals and conferences. Dr. Aldraihem serves as the universities coordinator for the award of King Abdulaziz & his Companions Foundation for Giftedness and Creativity.

Wael Akl is currently an assistant professor at Ain-Shams University – Cairo – Egypt. He is a co-founder of the sound and vibration lab at this institution. He has finished his M.Sc. degree in 1999 from the Design & Production Engineering Department at Ain-Shams University. He finished his 2nd M.Sc. and Ph.D. from the mechanical engineering department – University of Maryland – College Park – USA. He is working in the fields of structural dynamics, topology optimization, sensors and modeling in virtual reality. He has published several papers in the fields of topology optimization, developing sensors for morphing structures and noise control of underwater structures.

Amr Baz (http://www.enme.umd.edu/facstaff/fac-profiles/baz.html) earned his Ph.D. in Mechanical Engineering from University of Wisconsin at Madison in 1973. Currently, he is Professor of Mechanical Engineering at the University of Maryland in College Park, MD. He is also serving as the Director of the Smart Materials & Structures Research Center. Between 2001 and 2006, he served as the Director of the Small Smart Systems Center. His research interests include active and passive control of vibration and noise and virtual reality design of smart structures. He has published more than 140 papers in referred journals and holds 6 US patents. He is Fellow of the American Society of Mechanical Engineers, listed in Who's Who of American Inventors, and recipient of Engineering Alumni Association Outstanding Faculty Research Achievement Award. Dr. Baz serves on the editorial boards of journals of Vibration and Control, Thin-Walled Structures, Vehicle Noise & Vibration, Smart Structures & Systems, Mechanics of Advanced Materials and Structures, and Advances in Acoustics and Vibration.